

NanoSi low loss horizontal slot waveguides coupled to high Q ring resonators

Romain Guider,^{1*} Nicola Daldosso,¹ Alessandro Pitanti,¹ Emmanuel Jordana,² Jean-Marc Fedeli,² and Lorenzo Pavesi,¹

¹ Department of Physics, Università di Trento, Via Sommarive 14, I-38123 Povo (Trento), Italy

² CEA Léti-MINATEC, 17 rue des Martyrs, 38054 Grenoble Cedex 9, France

*guider@science.unitn.it

Abstract: Si-based horizontal slot waveguides coupled to ring resonators have been fabricated and characterised. The central layer of the slot has been filled by Silicon nanocrystals (Si-nc) obtained by deposition of silicon rich silicon oxide and then thermal annealing. A comparison of various deposition and annealing parameters to form the Si-nc is performed. Propagation losses as low as 3 dB/cm and ring resonator quality factor of 30,000 have been achieved at 1550 nm.

©2009 Optical Society of America

OCIS codes: (230.7370) Waveguides; (230.5750) Resonators; (230.4555) Coupled resonators

References and links

1. Proceeding of the IEEE special issue “*Silicon Photonics*,” Vol. **97**, No. 7 (July 2009).
2. Y. Vlasov, and S. McNab, “Losses in single-mode silicon-on-insulator strip waveguides and bends,” *Opt. Express* **12**(8), 1622–1631 (2004).
3. K. Yamada, T. Tsuchizawa, T. Watanabe, J. Takahashi, E. Tamechika, M. Takahashi, S. Uchiyama, H. Fukuda, T. Shoji, S. Itabashi, and H. Morita, “Microphotonic devices based on silicon wire waveguiding system,” *IEICE Trans. Electron.* **E 87–C**, 351–357 (2004).
4. S. McNab, N. Moll, and Y. Vlasov, “Ultra-low loss photonic integrated circuit with membrane-type photonic crystal waveguides,” *Opt. Express* **11**(22), 2927–2939 (2003).
5. V. R. Almeida, Q. Xu, C. A. Barrios, and M. Lipson, “Guiding and confining light in void nanostructure,” *Opt. Lett.* **29**(11), 1209–1211 (2004).
6. C. A. Barrios, “High performance all-optical silicon microswitch,” *Electron. Lett.* **40**(14), 862–863 (2004).
7. C. A. Barrios, B. Sánchez, K. B. Gylfason, A. Griol, H. Sohlström, M. Holgado, and R. Casquel, “Demonstration of slot-waveguide structures on silicon nitride / silicon oxide platform,” *Opt. Express* **15**(11), 6846–6856 (2007).
8. M. Lohmeyer, “*Guided waves in rectangular integrated magneto-optic devices*” (PhD thesis, 1999). www.home.math.utwente.nl/~hammer/Papers/phdth.pdf
9. A. Farjadpour, D. Roundy, A. Rodriguez, M. Ibanescu, P. Bermel, J. D. Joannopoulos, S. G. Johnson, and G. Burr, “Improving accuracy by subpixel smoothing in FDTD,” *Opt. Lett.* **31**, 2972–2974 (2006).
10. P. Sanchis, J. Blasco, A. Martinez, and J. Marti, “Design of silicon-based slot waveguide configurations for optimum nonlinear performance,” *J. Lightwave Technol.* **25**(5), 1298–1305 (2007).
11. Y. Lebour, R. Guider, E. Jordana, J.-M. Fedeli, P. Pellegrino, S. Hernandez, B. Garrido, N. Daldosso, and L. Pavesi, “High quality coupled ring resonators based on silicon clusters slot waveguide,” *Proc. of 5th IEEE Int. Conf. on Group IV Photonics*, 215–217 (2008).
12. N. Daldosso, and L. Pavesi, “NanoSilicon for Photonics,” *Laser Photonics Rev.* **3**, 508–534 (2009).
13. L. Pavesi, “Silicon-Based Light Sources for Silicon Integrated Circuits,” *Adv. Opt. Technol.* **2008**, 416926 (2008).
14. R. Spano, N. Daldosso, M. Cazzanelli, L. Ferraioli, L. Tartara, J. Yu, V. Degiorgio, E. Giordana, J. M. Fedeli, and L. Pavesi, “Bound electronic and free carrier nonlinearities in Silicon nanocrystals at 1550nm,” *Opt. Express* **17**(5), 3941–3950 (2009).
15. D. Navarro-Urrios, A. Pitanti, N. Daldosso, F. Gorbilleau, R. Rizk, G. Pucker, and L. Pavesi, “Quantification of the carrier absorption losses in Si-nanocrystal rich rib waveguides at 1.54 μm ,” *Appl. Phys. Lett.* **92**(5), 051101 (2008).
16. E. Jordana, J.-M. Fedeli, P. Lyan, J. P. Colonna, P. Gautier, N. Daldosso, L. Pavesi, Y. Lebour, P. Pellegrino, B. Garrido, J. Blasco, F. Cuesta-Soto, and P. Sanchis, “Deep-UV Lithography Fabrication of Slot Waveguides and Sandwiched Waveguides for Nonlinear Applications,” *Proc. of 4th IEEE Int. Conf. on Group IV Photonics*, 217–219 (2007).

17. S. Hernandez, P. Pellegrino, A. Martinez, Y. Lebour, B. Garrido, R. Spano, M. Cazzanelli, N. Daldosso, L. Pavesi, E. Jourdana, and J. M. Fedeli, "Linear and nonlinear optical properties of Si-nanocrystals in SiO₂ deposited by plasma-enhanced chemical-vapor deposition," *J. Appl. Phys.* **103**(6), 064309 (2008).
 18. R. Sun, P. Dong, N. N. Feng, C. Y. Hong, J. Michel, M. Lipson, and L. Kimerling, "Horizontal single and multiple slot waveguides: optical transmission at $\lambda = 1550$ nm," *Opt. Express* **15**(26), 17967–17972 (2007).
 19. K. Preston, and M. Lipson, "Slot waveguides with polycrystalline silicon for electrical injection," *Opt. Express* **17**(3), 1527–1534 (2009).
 20. M. Borselli, T. J. Johnson, and O. Painter, "Beyond the Rayleigh scattering limit in high-Q silicon microdisks: theory and experiment," *Opt. Express* **13**(5), 1515–1530 (2005).
 21. D. D. Smith, H. Chang, K. A. Fuller, A. T. Rosenberger, and R. W. Boyd, "Coupled-resonator-induced transparency," *Phys. Rev. A* **69**(6), 063804 (2004).
-

1. Introduction

Si photonics technology has made major advances in terms of design, fabrication, and device implementation [1]. At present days, it is at a turn-around point between technical development and commercial opportunities. The progress in fabrication technology has enabled the realization of photonic structures with deep-submicron feature size in ultrahigh-index contrast materials, most prominently, in silicon-on-insulator (SOI). In addition to waveguide structures such as silicon wires [2,3] and photonic crystal slab waveguides [4], slot waveguides have been proposed [5–7]. As silicon nanocrystals (Si-nc) embedded in SiO₂ have low refractive index (in the range 1.5-2.0 according to the Si excess), their use in conventional waveguides results in large cross-section and weak light confinement. The slot waveguide is a high-index contrast photonic structure with deep-submicron feature size that can help in solving such a problem. It consists of a thin layer of low-index material sandwiched by two high-index walls or layers (for vertical or horizontal configuration, respectively). Compared to conventional waveguides, where the main part of the optical field is confined within the high index core, a large fraction of the guided mode is in the low index layer. This occurs only for the polarization mode whose electric field is perpendicular to the slot interfaces: TM (transverse magnetic) polarization for the horizontal slot and TE (transverse electric) polarization for the vertical one. The field is affected by a discontinuity at the slot-wall interfaces and this increases the maxima of the optical field evanescent tails within the slot. If the slot width is smaller than the decay length of the field, it is possible to have a pile-up of the evanescent tails, thus enhancing the field intensity in this region with respect to the field confined in the walls.

A scheme of the horizontal slot waveguide, together with the electrical field profile of the slot-enhanced component (quasi-TM polarization) is shown in Fig. 1. The electric field profile has been calculated by using a fully vectorial commercial solver that implements the Wave Mode Matching (WMM) method. The software we have used is a freely-available solver [8]; additional simulations have been performed by using an FDTD code [9]. Design and optimization of the slot geometrical parameters to achieve minimum effective area (i.e. maximum field confinement) have been reported in Ref [10], where the influence of the refractive index in the slot region has been studied too. A minimum effective area of $0.1 \mu\text{m}^2$ was achieved with a slot waveguide width of 350 nm. This waveguide width ensures single mode TM propagation. However surface roughness causes significant losses at this width [11]. Thus to reduce the propagation losses, a width of about 500 nm has been chosen to fabricate the waveguides. At such a width, the second order TM mode is also present. However, it is extremely lossy being very close to the cut-off condition and spatially localized at the waveguide surface.

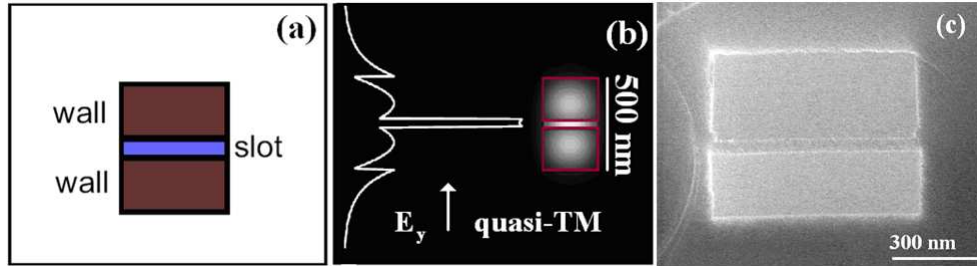


Fig. 1. (a) Horizontal slot waveguide scheme, (b) simulated field profile for the quasi-TM polarization and (c) SEM image (cross section) of a representative waveguide.

The idea of realizing nano-Si slot waveguides (i.e. waveguides where Si-nc embedded in SiO₂ are formed in the slot layer) is motivated by the unique properties of Si-nc [12]. The possibility of getting light amplification from Si-nc [13] and their non-linear properties at 1.5 μm (one order of magnitude larger than those of bulk Si [14]) would enable new photonic devices in which the characteristics of active optical materials can be efficiently exploited for modulation and switching, as proposed in ref [6]. However, the losses figure of nano-Si slot waveguides may be higher than that of SOI slot waveguides where bare silicon oxide is in the slot region. On one side the larger refractive index of nano-Si slot waveguide will decrease the refractive index contrast among the silicon walls and the slot region, which in turn will decrease the losses. On the other side, the composite nature of the material and the presence of excited carrier absorption can be detrimental for efficient optical propagation in nano-Si slot waveguide [15].

In this work, we experimentally study nano-Si slot waveguide based photonic structures, both waveguides and ring resonators. Horizontal slot waveguides filled with Si-nc have been realized and characterized in terms of propagation losses as a function of the layer deposition conditions (i.e. Si excess and annealing temperature). In a second part, we present experimental results of resonant optical cavities such single and double ring resonators coupled to the horizontal slot waveguides with very high quality factors.

2. Waveguides

The horizontal slot waveguide structure is composed by a Silicon-Rich-Silicon-Oxide (SRSO) layer (50-100 nm thick) placed between two silicon waveguides (200-300 nm thick). The starting wafer was a 200 mm SOI wafers with 220 nm thick crystalline silicon and 2 μm thick buried oxide (BOX). SRSO was deposited by plasma enhanced chemical vapour deposition (PECVD) by using different deposition conditions. Reference sample with SiO₂ has been deposited too. Various annealing treatments in inert (N₂) atmosphere (from 600 to 1000°C) were experienced to induce Si-nc formation. Then low loss hydrogenated amorphous silicon (a-Si) was deposited at 350°C and followed by 150 nm TEOS SiO₂ deposition acting as an hard mask [16]. 193 nm deep-UV lithography and hard mask etching was used to define sub-micrometer wide waveguides. The three layers (amorphous silicon, SRSO, and monocrystalline silicon) were etched sequentially down to the BOX. As a final step, the horizontal slot waveguides were covered by SiO₂. Scanning electron microscopy cross section of a typical horizontal slot waveguide is shown in Fig. 1. Its geometrical parameters are: 50 nm thick SRSO slot, 555nm waveguide height and 650 nm waveguide width. After an optimisation of the etching procedure, we have obtained horizontal slot waveguides of smaller width, about 500 nm [16].

To allow an easy and efficient in and out coupling of the light into the chip, they were coupled trough a tapering to a 2 μm wide waveguide. This maximizes the coupling of the light with the TM fundamental mode but prevents from any mode profiling measurements. A systematic study/design of the slot geometrical parameters has been already performed

aiming at optimizing the modal confinement factor [10], where the percentage of silicon excess inside the slot was studied in order to have the highest value of $n_g * FF$ for the waveguide, where n_g represents the group index and FF the filling factor of our slot waveguide.

A preliminary study on the material (in particular, correlation between refractive index and deposition parameters) has been performed in ref [17]. Here, a detailed investigation of the material (i.e. the SRSO layer) has been assessed in terms of waveguide losses. Different deposition conditions (i.e. Si excess in the SRSO layer, from 8% to 10%) and thermal annealing treatment (from 600 up to 1000 °C) have been used to correlate already optimized material properties [17] to optical losses within the horizontal slot waveguide configuration. It is worth to remind that high Si content for a fixed annealing temperature or high annealing temperature for a fixed Si excess imply a large refractive index (thus influencing both linear and nonlinear optical properties) [17]. We have compared the different PECVD deposition with a slot waveguide filled only of SiO₂ to differentiate the propagation losses due to the material rather than due to the slot structure.

Propagation losses have been determined from transmission measurements by using an optical tapered fiber mounted on a piezo-electric stage to butt-couple the input signal. To control the polarization, a fiber polarizer has been employed between the laser and the input fiber while a polarizer filter has been used in the collection system. Propagation losses of these waveguides have been measured at 1.55 μm. A dedicated layout structure allows the determination of the propagation losses independently on the coupling ones. It is shown in the inset of Fig. 2: it consists of a waveguide splitted into two channels. Since the two channels have different lengths, the ratio of the intensities at the outputs gives the linear propagation losses. Moreover, also the balance of the splitter has been carefully checked in waveguides with the same output path length.

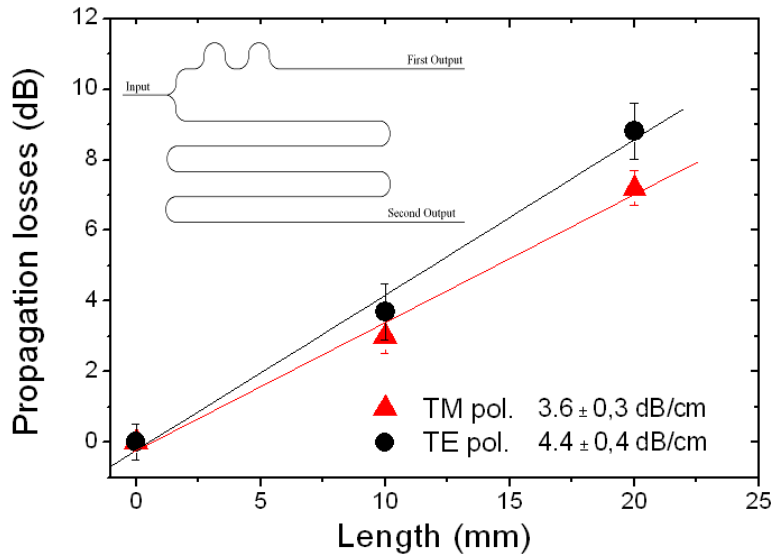


Fig. 2. Propagation losses of nano-Si slot waveguide with 8% Si excess annealed at 1000°C measured at 1550nm in TM and TE polarization. Inset: Top-view scheme of the waveguides on the mask.

Figure 2 shows a graph of the measurements for a slot waveguide with 8% Si excess annealed at 1000°C. Propagation losses of 3.6 dB/cm have been measured at 1550 nm for the quasi-TM polarization, while about 4.4 dB/cm for the quasi-TE polarization. Such optical loss values can be attributed to the fact that a large fraction of the optical mode is confined

within the slot which reduces the effects of the wall roughness and to the good layer interfaces obtained by the deposition technique used. This is supported by losses of 7.2 dB/cm found for the reference waveguide (slot waveguide with SiO₂). Similar results have been found in single slot waveguides formed by a-Si/SiO₂ [18,19].

In Table 1, a summary of the waveguide losses as a function of the material parameters is shown.

Table 1. Propagations losses for different slot waveguides for quasi-TE and -TM polarization at 1550 nm.

<i>Si excess</i>	<i>Annealing temperature (°C)</i>	<i>Propagation losses</i>	
		<i>quasi-TM (dB/cm)</i>	<i>quasi-TE (dB/cm)</i>
0% (TEOS SiO ₂)	600	7.2 ± 0.1	7.6 ± 0.8
8%	800	4.6 ± 0.3	5.4 ± 0.4
8%	1000	3.6 ± 0.3	4.4 ± 0.4
10%	600	4.7 ± 0.7	5.4 ± 0.6
10%	800	4.4 ± 0.7	-
10%	1000	3 ± 0.2	3.9 ± 1.1

Propagation losses decrease with increasing the Si excess or when the annealing temperature rises. It is worth noting that we were able to reach propagation losses as low as 3 dB/cm for quasi-TM polarization (sample with 10% of excess Si and annealed at 1000 °C), which is the best result reported for slot waveguides of such a small width. This is a consequence of the increasing of the refractive index as well as the result of a material optimization to minimize carrier absorption losses due to the Si-nc [15].

3. Ring Resonators

3.1 Quality factor and losses

We produced different ring resonators based on the nano-Si slot waveguides. A resonance of the ring occurs whenever $m\lambda_m = n_{eff}2\pi R$, where n_{eff} is the effective index of the waveguide, λ_m is the resonance wavelength, R is the ring radius and m is an arbitrary integer, also called the longitudinal mode number. It is worth noting that a change of either ring radius or refractive index implies a shift in the resonance wavelength. Testing of these is achieved by coupling a bus nano-Si slot waveguide to the ring (see SEM image in the inset of Fig. 3). A preliminary study on horizontal slot waveguides coupled to ring resonators as a function of the ring radius and ring-bus gap has been performed to optimize the bus-resonator coupling for TM polarization. Best results were found for ring-bus gaps of 250 nm independently of the ring radius [11]. Optical transmission spectra through the bus waveguide were measured in the range 1520–1620 nm by a tunable laser passed through a polarization controller and a tapered fiber.

Figure 3 (inset) shows the best transmission spectrum in term of quality factor for both TE and TM polarization of a ring ($R = 20 \mu\text{m}$) coupled to the bus waveguide by 250 nm wide gap of nano-Si slot waveguide. Since the coupling is optimised for the quasi-TM mode, resonances are observed for TM light and not for TE light. This indicates that no polarization conversion effects occur within the slot waveguide.

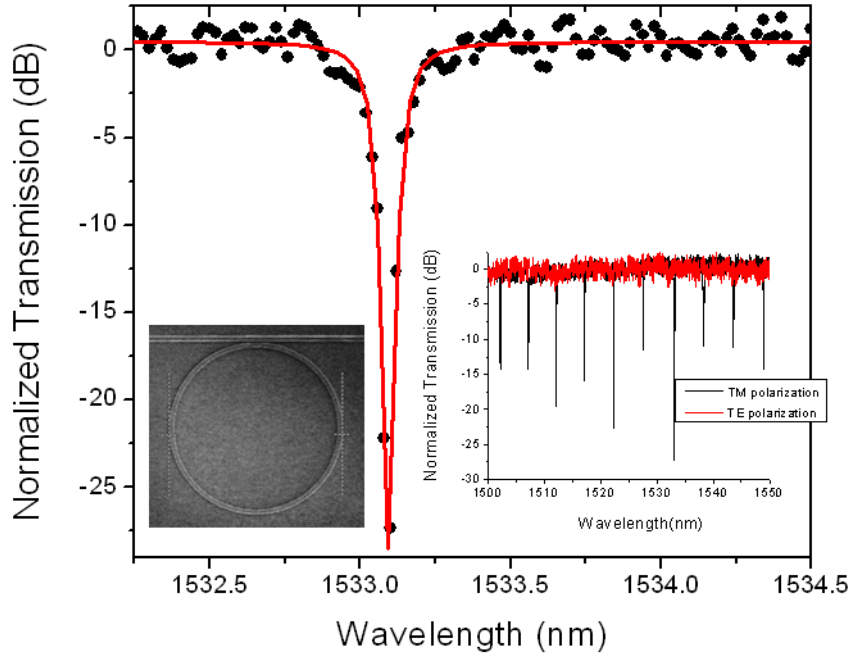


Fig. 3. Normalized transmission measurement of a ring resonator with $R = 20\mu\text{m}$ and a ring-bus gap of 250nm. A resonance at 1533.8nm is observed with a quality factor $Q = 30,000$. The red line is a lorentzian fit to the dat. (Inset-right) Full spectral interval results for both TE and TM polarization. (Inset-left) SEM image.

Figure 3 shows the detailed spectrum of the resonance at 1533.08 nm. A Lorentzian fit allows the extraction of significant parameters. The resonance extinction ratio is 27 dB. The 3dB bandwidth is $\Delta\lambda = 0.051 \pm 0.01$ nm. This corresponds to a quality factor $Q_{\text{factor}} = \lambda/\Delta\lambda = 30000 \pm 6000$ at 1533.08 nm. In smaller rings ($R = 10 \mu\text{m}$), Q_{factor} of about 20000 has been found. Free spectral range (*FSR*) of about 11 nm and 5.8 nm have been found for the $R = 10$ and 20 μm rings, respectively. Comparing our results with literature results, we found that Q factors of about 13000 have been reached in similar sized rings ($R = 10 \mu\text{m}$, 150 nm bus gap) [18], while Q factors of about 82000 have been obtained in larger rings ($R = 100 \mu\text{m}$) [19].

In order to compare the losses inside the cavity with the linear propagation losses, we have extracted from the Lorentzian fit parameters the “intrinsic quality factor” of the resonators. The total quality factor (Q_{tot}) can be represented, in a first approximation, as:

$$\frac{1}{Q_{\text{tot}}} = \frac{1}{Q_r} + \frac{1}{Q_{\text{coupl}}} \quad (1)$$

where Q_r is the intrinsic quality factor, whereas Q_{coupl} takes into account the losses due to the coupling with the bus waveguide. The latter can be extracted from the extinction ratio at the resonance (T_{min}), as [20]:

$$Q_{\text{coupl}} = \frac{2Q_{\text{tot}}}{1 - \sqrt{T_{\text{min}}}} \quad (2)$$

Once Q_r is known, the losses inside the ring α_r can be determined by:

$$\alpha_r = \frac{2\pi n_g}{\lambda Q_r} \quad (3)$$

where n_g is the group index.

Table 2 reports Q_r and α_r found in samples with and without Si-nc at different input powers. The measured Q factors are similar within the experimental errors bars independently of the Si-nc parameters.

Table 2. Q_r and α_r in coupled rings ($R = 20\mu\text{m}$) with and without Si-nc at different input powers at $\lambda = 1533\text{nm}$.

Slot waveguide filled by:	$P_{in} < 0.5\text{mW}$		$P_{in} = 3\text{mW}$	
	Q_r	α_r (dB/cm)	Q_r	α_r (dB/cm)
SiO_2	36100 ± 6000	17 ± 3	39000 ± 6000	16 ± 3
Si-nc	35600 ± 6000	18 ± 3	39600 ± 6000	16 ± 3

The values of α_r are larger than those found in the correspondent straight waveguides (see Table 1) because they include both linear and bending-induced contributions as well as mode-mismatch losses at the coupling region. Losses inside the rings are similar for both samples. This is in contrast with the linear losses, which differ by about 3-4 dB/cm. It looks like that the processing used to form the rings causes additional losses which mask the role of the slot region composition in α_r .

In addition, the large error bars in the Q_{factor} measurements causes an indetermination on α_r which is of the same extent as the difference of propagation losses between the waveguides with and without Si-nc.

3.2 Effect of Si-nc in ring resonators

Nevertheless, Si-nc in the ring resonators are still clearly affecting their properties. Indeed, a shift of the resonance peak position with increasing the light power in the nano-Si and not in the silica ring resonators is observed (Fig. 4).

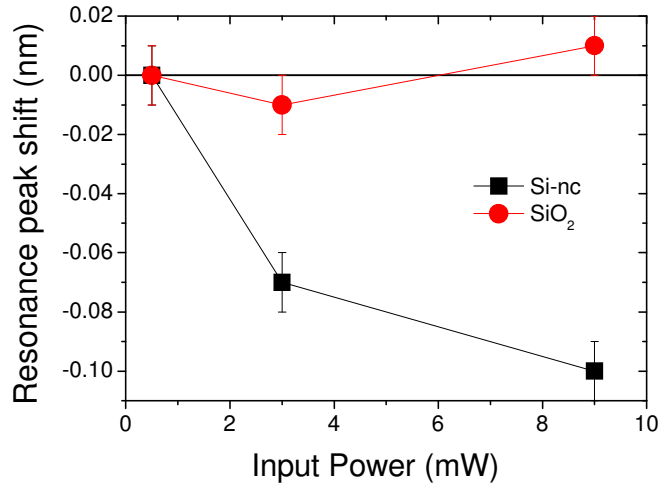


Fig. 4. Shift of the resonance peak position as a function of the input power.

As we observe a blue shift of the resonance peak position, the effective index of the propagating mode is decreased ($\Delta n = 10^{-4}$) due to free carrier refraction effects in Si-nc. Free Carriers are generated by two photon absorption which is sizeable in Si-nc [14]. Usually, free carriers cause absorption losses in Si-nc waveguides of a few dB/cm [15]. This is observed in Table 2 because it is within the errors bars. Non-linear optical effects due to free carriers

cannot be the responsible of such a behavior because the power density in the slot waveguides (about few hundreds of kW/cm²) will induce a wavelength shift of the order of 10⁻⁶ μm [14].

3.3 Group index

From the FSR, it is possible to deduce the group index n_g by:

$$FSR = \frac{\lambda^2}{n_g(\lambda) \times 2\pi R} \quad (4)$$

for the quasi-TM modes in the wavelength range from 1500 to 1550 nm. In Fig. 5, we compare both the values of n_g measured experimentally and the values found by simulations.

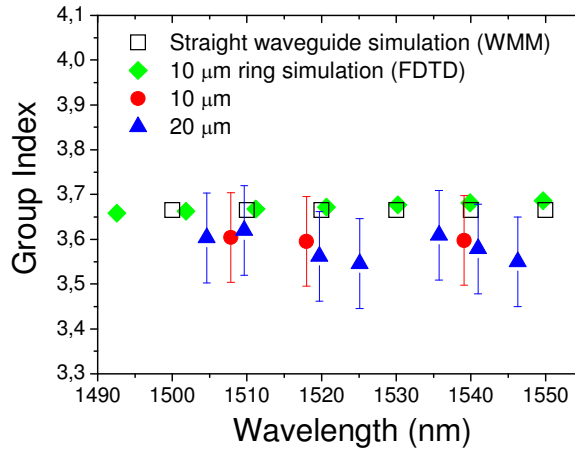


Fig. 5. Group index measurements and simulations.

The calculated values, included for comparison, were determined by:

$$n_g = n_{eff}(\lambda) - \lambda \frac{dn_{eff}(\lambda)}{d\lambda} \quad (5)$$

where the effective indices are calculated from the slot-waveguide parameters with a full-vectorial WMM solver. The simulated values of n_g have been obtained for a straight slot waveguide and a 10 μm radius ring by a FDTD code, where Eq. (4) has been used. Very good agreement is found between the experimental values (which are the same within the error bars) and with the simulated ones (less than 2% difference). This small difference has been found also in Ref [18]. It can be due either to the uncertainty in the fabricated slot waveguide size and indices or to the fact that the profile of the refraction index in the slot region is supposed to be flat, which might be not the case.

3.4 Double rings

Double coupled rings have been realized to increase the field enhancement of the optical cavity. This would allow the build-up of the intensity inside the optical resonator, thus improving the optical fluences at values sufficient to giving rise to optical non-linear effects. In Fig. 6, the resonances of single and double ring resonators are compared. The splitting of the resonances demonstrates the good coupling between the two-rings. In fact, the whispering

gallery modes in coupled microresonators are split symmetrically when the individual resonators have the same optical path length (OPL). It's due to the fact that the light must pass through a coupler twice, acquiring a net π phase shift before interfering with the light in the first resonator. When the OPL's of the two rings is the same, such that $\Phi_1 = \Phi_2 = \Phi$ (where Φ is the round-trip phase shift) the absorbance presents a minimum at the single-ring resonances ($\Phi_{\text{mod}}(2\pi) = 0$), resulting in the peak splitting [21]. For these double ring resonators, we found very high Q-factors: around 32000 for $R = 10 \mu\text{m}$, which is larger than the corresponding single ring Q of about 20000.

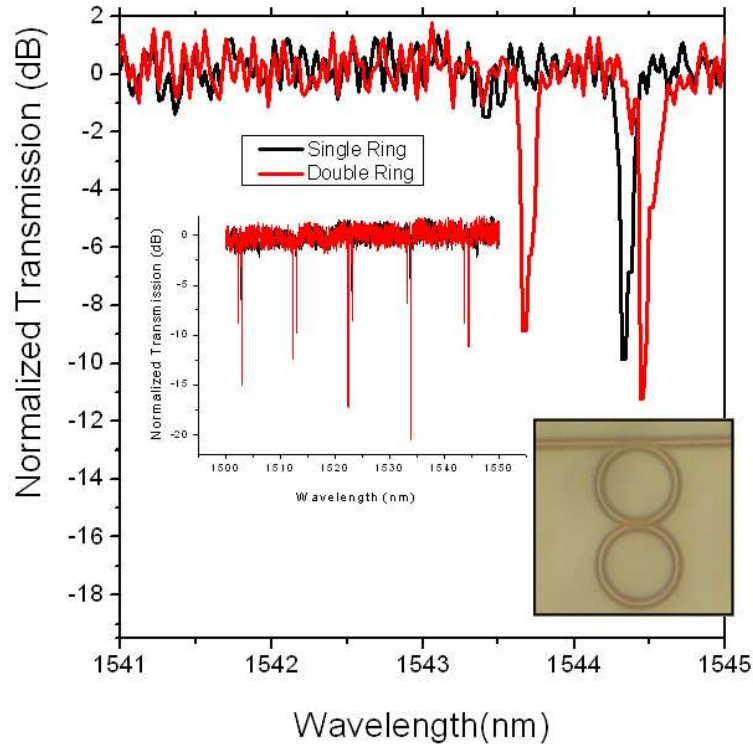


Fig. 6. Resonance at 1543.97nm for double (red) and at 1544.3nm for single (black) ring ($R = 10\mu\text{m}$ with gaps of 250nm). Inset left: transmission spectra in a large wavelength range (1500-1550nm). Inset right: Optical image of the $R = 10\mu\text{m}$ doubled coupled ring resonators.

4. Conclusion

We have demonstrated low losses nano-Si slot waveguides and high-quality factor coupled ring resonators. The importance of this work relies on the fact that by optimizing the annealed SRSO (i.e. Si-nc) in the slot, we have significantly reduced the propagation losses and at the same time we can add new functionalities related to the Si-nc optical properties (i.e. light emission and/or non-linear optical effects). The high-quality factors demonstrated in single and double ring resonators, if associated to the sizeable non-linear effect of nano-Si in the slot, can enable all optical switches and tunable telecommunications filters.

Acknowledgements

Financial support by EC under project 017158-PHOLOGIC is acknowledged.